

Measurements of G_E^n/G_M^n from the ${}^2\text{H}(\vec{e}, e'\vec{n}){}^1\text{H}$ Reaction to $Q^2 = 1.45$ (GeV/c) 2

R. Madey,^{1,2} A. Yu. Semenov,¹ S. Taylor,³ B. Plaster,³ A. Aghalaryan,⁴ E. Crouse,⁵ G. MacLachlan,⁶ S. Tajima,⁷ W. Tireman,¹ Chenyu Yan,¹ A. Ahmidouch,⁸ B. D. Anderson,¹ H. Arenhövel,⁹ R. Asaturyan,⁴ O. Baker,¹⁰ A. R. Baldwin,¹ D. Barkhuff,^{3,*} H. Breuer,¹¹ R. Carlini,² E. Christy,¹⁰ S. Churchwell,^{7,†} L. Cole,¹⁰ S. Danagoulian,^{2,8} D. Day,¹² T. Eden,^{1,10,‡} M. Elaasar,¹³ R. Ent,² M. Farkhondeh,³ H. Fenker,² J. M. Finn,⁵ L. Gan,¹⁰ K. Garrow,² P. Gueye,¹⁰ C. R. Howell,⁷ B. Hu,¹⁰ M. K. Jones,² J. J. Kelly,¹¹ C. Keppel,¹⁰ M. Khandaker,¹⁴ W.-Y. Kim,¹⁵ S. Kowalski,³ A. Lai,¹ A. Lung,² D. Mack,² D. M. Manley,¹ P. Markowitz,¹⁶ J. Mitchell,² H. Mkrtchyan,⁴ A. K. Opper,⁶ C. Perdrisat,⁵ V. Punjabi,¹⁴ B. Raue,¹⁶ T. Reichelt,¹⁷ J. Reinhold,¹⁶ J. Roche,⁵ Y. Sato,¹⁰ N. Savvinov,¹¹ I. A. Semenova,¹ W. Seo,¹⁵ N. Simicevic,¹⁸ G. Smith,² S. Stepanyan,^{4,15} V. Tadevosyan,⁴ L. Tang,¹⁰ P. E. Ulmer,¹⁹ W. Vulcan,² J. W. Watson,¹ S. Wells,¹⁸ F. Wesselmann,¹² S. Wood,² Chen Yan,² S. Yang,¹⁵ L. Yuan,¹⁰ W.-M. Zhang,¹ H. Zhu,¹² and X. Zhu¹⁰

(The Jefferson Laboratory E93-038 Collaboration)

¹*Kent State University, Kent, Ohio 44242*

²*Thomas Jefferson National Accelerator Facility, Newport News, Virginia 23606*

³*Massachusetts Institute of Technology, Cambridge, Massachusetts 02139*

⁴*Yerevan Physics Institute, Yerevan 375036, Armenia*

⁵*The College of William and Mary, Williamsburg, Virginia 23187*

⁶*Ohio University, Athens, Ohio 45701*

⁷*Duke University and TUNL, Durham, North Carolina 27708*

⁸*North Carolina A&T State University, Greensboro, North Carolina 27411*

⁹*Johannes Gutenberg-Universität, D-55099 Mainz, Germany*

¹⁰*Hampton University, Hampton, Virginia, 23668*

¹¹*University of Maryland, College Park, Maryland 20742*

¹²*University of Virginia, Charlottesville, Virginia 22904*

¹³*Southern University at New Orleans, New Orleans, Louisiana 70126*

¹⁴*Norfolk State University, Norfolk, Virginia 23504*

¹⁵*Kyungpook National University, Taegu 702-701, Korea*

¹⁶*Florida International University, Miami, Florida 33199*

¹⁷*Rheinische Friedrich-Wilhelms-Universität, D-53115 Bonn, Germany*

¹⁸*Louisiana Tech University, Ruston, Louisiana 71272*

¹⁹*Old Dominion University, Norfolk, Virginia 23529*

(Dated: September 26, 2018)

We report new measurements of the ratio of the electric form factor to the magnetic form factor of the neutron, G_E^n/G_M^n , obtained via recoil polarimetry from the quasielastic ${}^2\text{H}(\vec{e}, e'\vec{n}){}^1\text{H}$ reaction at Q^2 values of 0.45, 1.13, and 1.45 (GeV/c) 2 with relative statistical uncertainties of 7.6 and 8.4% at the two higher Q^2 points, which were not reached previously via polarization measurements. Scale and systematic uncertainties are small.

PACS numbers: 14.20.Dh, 13.40.Gp, 25.30.Bf, 24.70.+s

The nucleon elastic electromagnetic form factors are fundamental quantities needed for an understanding of nucleon and nuclear structure. The evolution of the electric and magnetic form factors with Q^2 , the square of the four-momentum transfer, is related to the charge and current distributions within the nucleon. Precision measurements of the electromagnetic form factors are important for tests of non-perturbative quantum chromodynamics (QCD) either on the lattice or in models. Measurements

of the neutron electric form factor, G_E^n , have been impeded by the lack of a free neutron target and the small value of G_E^n relative to the neutron magnetic form factor, G_M^n ; however, with the advent of high duty-factor polarized electron beam facilities, experiments employing recoil polarimeters [1, 2], polarized ${}^3\text{He}$ targets [3, 4, 5], and polarized deuterium targets [6, 7] have yielded the first precision measurements of G_E^n . These polarization measurements of G_E^n are limited to $Q^2 \leq 0.67$ (GeV/c) 2 and are, within errors, consistent with the Galster parameterization [8]. In addition to polarization measurements, G_E^n has been extracted from a theoretical analysis of the deuteron quadrupole form factor [9] for Q^2 values up to 1.6 (GeV/c) 2 .

In the plane-wave approximation, the recoil polarization produced by a longitudinally polarized electron beam in quasielastic electron-neutron scattering is re-

*Present Address: Renaissance Technologies, 600 Route 25A, East Setauket, New York 11733.

†Present Address: Dept. of Physics and Astronomy, University of Canterbury, Private Bag 4800, Christchurch 8020, New Zealand.

‡Present Address: Atmospheric Chemistry Division, National Center for Atmospheric Research, Boulder, Colorado 80307.

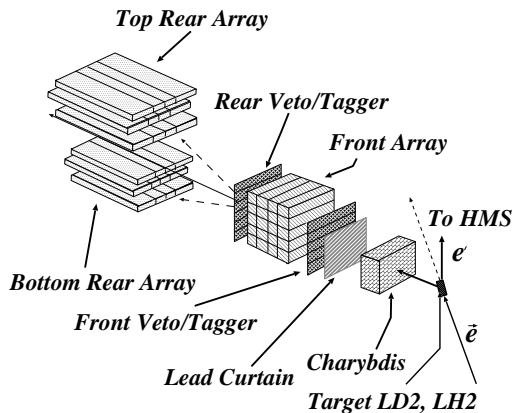


FIG. 1: A schematic diagram of the polarimeter.

stricted to the scattering plane [10, 11]: The longitudinal component, $P_{L'}$, and the transverse (sideways) component, $P_{S'}$, are parallel and perpendicular, respectively, to the recoil neutron's momentum vector. In terms of G_E^n and G_M^n , $P_{S'}$ and $P_{L'}$ can be written as

$$P_{S'}/P_L = -K_S G_E^n G_M^n / I_0, \quad (1)$$

$$P_{L'}/P_L = K_L (G_M^n)^2 / I_0, \quad (2)$$

where P_L is the electron beam polarization, $I_0 \equiv (G_E^n)^2 + K_0 (G_M^n)^2$, and K_S , K_L , and K_0 are kinematic functions of the electron scattering angle, θ_e , and Q^2 . Measurements of $P_{S'}$ and $P_{L'}$ via a secondary analyzing reaction permit an extraction of the ratio of G_E^n to G_M^n ; a significant advantage of this technique is that P_L and the analyzing power of the secondary reaction cancel in the polarization ratio $P_{S'}/P_{L'}$. Also, for quasifree emission, Arenhövel [12] demonstrated that $P_{S'}$ and $P_{L'}$ are insensitive to final state interactions (FSI), meson exchange currents (MEC), isobar configurations (IC), and to theoretical models of deuteron structure. In this Letter, we report new measurements of G_E^n/G_M^n obtained via recoil polarimetry from the quasielastic ${}^2\text{H}(\vec{e}, e'\vec{n}){}^1\text{H}$ reaction at three central Q^2 values of 0.45, 1.15, and 1.47 $(\text{GeV}/c)^2$.

Our measurements were carried out in Hall C of the Thomas Jefferson National Accelerator Facility. The experimental arrangement with an isometric view of our polarimeter is shown in Fig. 1. A beam of longitudinally polarized electrons (with a typical polarization of 80%) scattered quasielastically from a neutron in a 15-cm liquid deuterium target. A scattered electron was detected in the High Momentum Spectrometer (HMS) in coincidence with the recoil neutron. The neutron polarimeter (NPOL) was used to measure the up-down scattering asymmetry from the transverse component of the recoil neutron polarization presented to the polarimeter. To permit measurements of the up-down scattering asymmetry from different combinations of $P_{S'}$ and $P_{L'}$, a dipole magnet (Charybdis) located in front of the polarimeter precessed the recoil neutron's polarization vector through an angle χ .

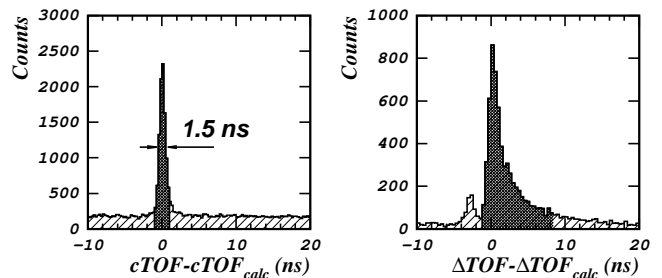


FIG. 2: Typical time-of-flight spectra for $Q^2 = 1.15$ $(\text{GeV}/c)^2$. The dark-shaded regions indicate the selected portions of the spectra.

The polarimeter consisted of a total of 44 plastic scintillation detectors. To achieve luminosities of $\sim 3 \times 10^{38}$ $\text{cm}^{-2} \text{s}^{-1}$, the front array was segmented into 20 detectors $[100 \text{ cm} \times 10 \text{ cm} \times 10 \text{ cm}]$. Top and bottom rear arrays were shielded from the direct path of particles from the target. Each rear array consisted of 6 “20-in” detectors $[101.6 \text{ cm} \times 50.8 \text{ cm} \times 10.16 \text{ cm}]$ and 6 “10-in” detectors $[101.6 \text{ cm} \times 25.4 \text{ cm} \times 10.16 \text{ cm}]$. A double layer of “veto/tagger” detectors (each 0.64-cm thick) directly ahead of and behind the front array identified incoming and scattered charged particles. A 10-cm lead curtain attenuated the flux of electromagnetic radiation and charged particles incident on the polarimeter. The flight path from the center of the target to the center of the front array was 7.0 m, and the mean flight path from the front array to the rear array was 2.5 m.

For a fixed neutron scattering angle of 46.0° , central Q^2 values of 0.45 and 1.47 $(\text{GeV}/c)^2$ were associated with beam energies of 0.884 and 3.40 GeV, respectively, and electron scattering angles of 52.7° and 23.6° , respectively. The measurement conducted at a central Q^2 value of 1.15 $(\text{GeV}/c)^2$ was associated with two beam energies of 2.33 and 2.42 GeV and electron scattering angles of 30.8° and 30.1° , respectively. We conducted asymmetry measurements with the polarization vector precessed through $\chi = \pm 40^\circ$ at each of our Q^2 points; in addition, at $Q^2 = 1.15$ and 1.47 $(\text{GeV}/c)^2$, we conducted asymmetry measurements with the polarization vector precessed through $\chi = 0^\circ, \pm 90^\circ$. The acceptance-averaged values of Q^2 are: $\langle Q^2 \rangle = 0.45, 1.13, \text{ and } 1.45$ $(\text{GeV}/c)^2$.

Typical time-of-flight spectra are shown in Fig. 2. The left panel is an HMS-NPOL coincidence time-of-flight spectrum. We compared the measured time-of-flight, $c\text{TOF}$, with the time-of-flight calculated from electron kinematics and offsets determined by a calibration procedure; the result is centered on zero with a FWHM of approximately 1.5 ns. The right panel is the time-of-flight spectrum between a neutron event in the front array and an event in the top or bottom rear array. We compared this measured time-of-flight, ΔTOF , with the time-of-flight calculated for elastic np scattering. Variations with respect to a nominal 2.5 m flight path were compensated. The tail on the slow side is due to Fermi motion in carbon and nuclear reactions, and the secondary peak at

~ -2.5 ns is the result of π^0 production in the front array. To extract the physical scattering asymmetry, we calculated the cross ratio, r , which is defined to be the ratio of two geometric means, $(N_U^+ N_D^-)^{1/2}$ and $(N_U^- N_D^+)^{1/2}$, where $N_U^+(N_D^-)$ is the yield in the Δ TOF peak for neutrons scattered up(down) when the beam helicity was positive(negative); the yields, corrected for background, were obtained by peak fitting. The physical scattering asymmetry is then given by $(r - 1)/(r + 1)$. The merit of the cross ratio technique [13] is that the neutron polarimeter results are independent of the luminosities for positive and negative helicities, and the efficiencies and acceptances of the top and bottom halves of the polarimeter. Beam charge asymmetries (of typically 0.1%) and detector threshold differences cancel in the cross ratio.

To account for the finite experimental acceptance and nuclear physics effects such as FSI, MEC, and IC, we averaged Arenhövel's theoretical ${}^2\text{H}(\vec{e}, e'\vec{n}){}^1\text{H}$ calculations [14] over the experimental acceptance. These calculations include leading-order relativistic contributions to a non-relativistic model of the deuteron as an n - p system, employ the Bonn R -space NN potential [15] for the inclusion of FSI, and include MEC and IC. Other realistic potentials (e.g., the Argonne V18 [16]) give essentially the same results. The theoretical values of the recoil polarization were calculated over a kinematic grid; during the averaging procedure, the recoil polarization was computed via multidimensional interpolation between the grid elements.

To average these theoretical calculations over the experimental acceptance, we prepared two independent simulation programs. First, we developed the GENGEN Monte Carlo simulation program, which includes an event generator and detailed models of the electron spectrometer and the neutron polarimeter. GENGEN reproduces experimental kinematic distributions and models the response of the polarimeter. Second, we developed a program that used the kinematics of the reconstructed quasielastic events from the experimental data to compute the recoil polarization for each event used in the data analysis; the advantage of this method is that it does not require a model of the experimental acceptance.

For the first-pass analysis, the simulation programs used theoretical calculations that assumed the Galster parameterization for G_E^n with different multiplicative factors. We determined via simulation the optimal factor for each Q^2 that provided the best agreement between the simulated polarization ratios and the experimental asymmetry ratios. Next we fitted the current world data [1, 2, 4, 5, 6, 7, 9, 17] and our first-pass acceptance and nuclear physics corrected results for G_E^n to a Galster parameterization with two free parameters. Then we repeated the simulations using new theoretical calculations that assumed this modified Galster parameterization for G_E^n . As in the first-pass analysis, we determined via simulation the optimal factor that provided the best agreement between simulation and experiment. The differences between these analyses were negligible, and the

TABLE I: Estimated systematic uncertainties in $\Delta g/g$ [%].

Source	$\langle Q^2 \rangle$ [(GeV/c) 2]				
	0.45 ^a	1.13 ^a	1.13 ^b	1.45 ^a	1.45 ^b
Beam Polarization	1.4	0.8	0.4	1.7	0.3
Charge Exchange	<0.01	0.02	0.06	<0.01	0.2
Depolarization	<0.1	<0.1	0.2	0.1	0.6
Positioning/Traceback	0.2	0.3	0.3	0.4	0.4
Precession Angle	1.1	0.3	0.1	0.5	0.1
Radiative Corrections	0.7	0.1	0.1	0.05	0.05
Total of Above Sources	1.9	0.9	0.5	1.8	0.8

^a $\chi = \pm 40^\circ$ precession.

^b $\chi = 0^\circ, \pm 90^\circ$ precession.

results from the two simulation programs agreed to better than two percent.

The estimated values of the systematic uncertainties are listed in Table I. A significant advantage of our experimental technique is that the scale and systematic uncertainties are small; the analyzing power of the polarimeter cancels in the polarization ratio, and the beam polarization, P_L , also cancels as it varied little during sequential measurements of the scattering asymmetries. We measured the beam polarization with a Møller polarimeter [18], and changes in P_L were typically on the order of one to two percent. The helicity of the beam was reversed at a frequency of 30 Hz to eliminate instrumental asymmetries.

A false asymmetry or a dilution of the asymmetry may arise from the two-step process ${}^2\text{H}(\vec{e}, e'\vec{p}){}^1\text{H} + \text{Pb}(\vec{p}, \vec{n})$; the contamination from this process was assessed by running with a liquid hydrogen target. The contamination levels are negligible ($\lesssim 0.3\%$) for $\chi = \pm 40^\circ$ and $\pm 90^\circ$ at all of our Q^2 points, and for $\chi = 0^\circ$, the contamination levels are $\sim 0.3\%$ and $\sim 3\%$ at $\langle Q^2 \rangle = 1.13$ and 1.45 (GeV/c) 2 , respectively; accordingly, we have not corrected our $\langle Q^2 \rangle = 0.45$ and 1.13 (GeV/c) 2 data for contamination from this two-step process. The net correction obtained for the analysis of all of the data for $\langle Q^2 \rangle = 1.45$ (GeV/c) 2 [viz., for $\chi = 0^\circ, \pm 40^\circ$, and $\pm 90^\circ$] amounted to $1.3 \pm 0.1\%$. In addition to charge-exchange reactions in the lead curtain, the flux of neutrons entering the polarimeter may be depolarized as a result of nuclear interactions in the lead curtain. Depolarization processes were simulated in GENGEN using a spin-dependent multiple-scattering algorithm employing quasifree scattering from a Fermi gas. The effects of depolarization cancel in the polarization ratio, and the residual non-cancellation effect upon g of less than 0.6% is included in the systematic uncertainty.

Afanasev *et al.* [19] calculated radiative corrections to the polarization-transfer coefficients, $P_{S'}/P_L$ and $P_{L'}/P_L$. The primary effect is depolarization of the electron such that both polarization-transfer coefficients should be increased by $\sim 1.9\%$, $\sim 3.7\%$, and $\sim 4.4\%$ at $\langle Q^2 \rangle = 0.45, 1.13$, and 1.45 (GeV/c) 2 , respectively; however, these effects nearly cancel in the polarization ratio

TABLE II: Results for $g = G_E^n/G_M^n$ and G_E^n .

$\langle Q^2 \rangle$ [(GeV/c) 2]	$g = G_E^n/G_M^n$	$G_M^n/\mu_n G_D$ [20]	G_E^n
0.447	$-0.0761 \pm 0.0083 \pm 0.0021$	1.003 ± 0.006	$0.0550 \pm 0.0060 \pm 0.0016$
1.132	$-0.131 \pm 0.010 \pm 0.003$	1.057 ± 0.017	$0.0394 \pm 0.0029 \pm 0.0012$
1.450	$-0.190 \pm 0.016 \pm 0.004$	1.044 ± 0.024	$0.0411 \pm 0.0035 \pm 0.0013$

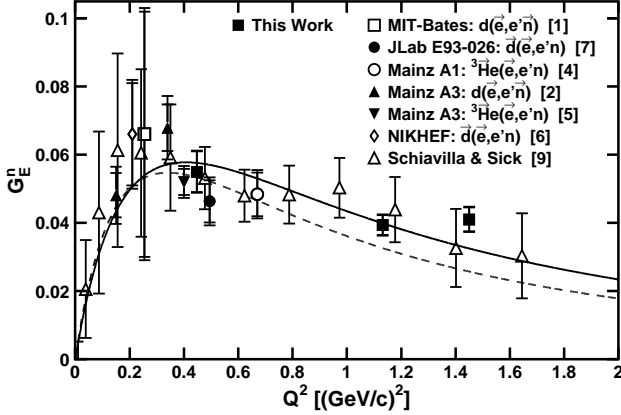


FIG. 3: The current world data on G_E^n versus Q^2 extracted from polarization measurements and an analysis of the deuteron quadrupole form factor [1, 2, 4, 5, 6, 7, 9]. The Galster parameterization [8] is the dashed line, and our two-parameter Galster fit (see text) is the solid line.

such that the net effect upon g is small at $\langle Q^2 \rangle = 0.45$ (GeV/c) 2 and negligible at the two higher Q^2 points.

The values of g and G_E^n that we report are listed in Table II. To determine our values for G_E^n , we used the best-fit values for G_M^n (listed in Table II) obtained using the methods described in [20]. The new fit omits the data of [21, 22] and includes the recent data of Xu *et al.* [23]. The results are similar to those obtained by Friedrich and Walcher [24] using a parameterization designed to investigate the role of the pion cloud. The fit is also similar to that of Kubon *et al.* [25] within their range of Q^2 , but extends to larger Q^2 . For g and G_E^n , the first set of errors is statistical, and the second set is systematic. The quoted systematic uncertainties for g include a 2% uncertainty that results when a different selection of runs is used for the time calibration. To obtain the systematic uncertainties for G_E^n , the relative uncertainties in G_M^n were added quadratically to the systematic uncertainties listed in Table I and the 2% time calibration uncertainty.

Our values for G_E^n are plotted in Fig. 3 together with the current world data on G_E^n [1, 2, 4, 5, 6, 7, 9] extracted from polarization measurements and an analysis of the deuteron quadrupole form factor. We fitted these data and the G_E^n slope at the origin as measured via low-energy neutron scattering from electrons in heavy atoms [17] to a Galster parameterization: $G_E^n = -a\mu_n\tau G_D/(1+b\tau)$, where $\tau = Q^2/4M_n^2$, $G_D = (1+Q^2/\Lambda^2)^{-2}$, and $\Lambda^2 = 0.71$ (GeV/c) 2 . Our best-fit parameters are $a = 0.888 \pm 0.023$ and $b = 3.21 \pm 0.33$.

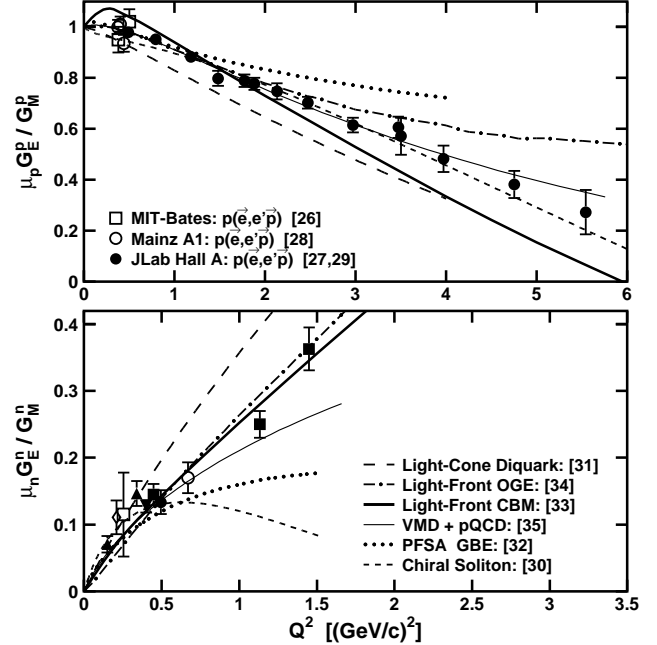


FIG. 4: Predictions of selected models (see text) for $\mu_p G_E^p/G_M^p$ and $\mu_n G_E^n/G_M^n$ compared with proton [26, 27, 28, 29] and neutron [1, 2, 4, 5, 6, 7] data. The neutron data symbols are the same as in Fig. 3.

Polarization measurements of G_E^p/G_M^p [26, 27, 28, 29] and G_E^n/G_M^n [1, 2, 4, 5, 6, 7, 9] are compared with predictions of selected models in Fig. 4. The chiral soliton model [30] reproduces the dramatic linear decrease observed in $\mu_p G_E^p/G_M^p$ for $1 < Q^2 < 6$ (GeV/c) 2 ; however, this model fails to reproduce the neutron data at large Q^2 . The light-cone diquark model [31] achieves qualitative agreement with the low Q^2 proton and neutron data; however, at high Q^2 , it lies below(above) the proton(neutron) data. A calculation using the point-form spectator approximation (PFSA) with pointlike constituent quarks and a Goldstone boson exchange interaction fitted to the meson and baryon spectrum [32] also achieves qualitative agreement with the low Q^2 proton and neutron data; however, it, too, fails to describe the high Q^2 proton and neutron data. A light-front calculation using pointlike constituent quarks surrounded by a cloud of pions [33] describes the neutron data, but falls below the proton data at high Q^2 . A one-gluon exchange light-front calculation using constituent quark form factors fitted to $Q^2 < 1$ (GeV/c) 2 data [34] agrees with the neutron data, but deviates from the proton data above

$Q^2 \sim 3.5$ (GeV/c)². Finally, fits that couple vector meson dominance with the predictions of perturbative QCD [35] agree with the entire range of the proton data, but fall below the neutron data above $Q^2 \sim 1.2$ (GeV/c)².

A successful model of confinement must be able to predict both neutron and proton electromagnetic form factors simultaneously. Although these models achieve qualitative agreement with the proton data, the neutron electric form factor is especially sensitive to small components of the nucleon wave function and differences between model predictions for G_E^n tend to increase rapidly with Q^2 . Our new G_E^n data for $0.5 < Q^2 < 1.5$ (GeV/c)²

provide a challenging test for confinement models and invite extensions to higher Q^2 .

We thank the TJNAF Hall C scientific and engineering staff for their outstanding support. Also, we thank A. Afanasev for providing calculations of the radiative correction uncertainties. This work was supported in part by the National Science Foundation, the U.S. Department of Energy, and the Deutsche Forschungsgemeinschaft. The Southeastern Universities Research Association (SURA) operates the Thomas Jefferson National Accelerator Facility under the U.S. Department of Energy contract DE-AC05-84ER40150.

-
- [1] T. Eden *et al.*, Phys. Rev. C **50**, R1749 (1994).
 [2] C. Herberg *et al.*, Eur. Phys. J. A **5**, 131 (1999) applies FSI corrections to M. Ostrick *et al.*, Phys. Rev. Lett. **83**, 276 (1999).
 [3] M. Meyerhoff *et al.*, Phys. Lett. B **327**, 201 (1994).
 [4] J. Bermuth *et al.*, Phys. Lett. B **564**, 199 (2003) updates D. Rohe *et al.*, Phys. Rev. Lett. **83**, 4257 (1999).
 [5] J. Golak, G. Ziemer, H. Kamada, H. Witala, and W. Glöckle, Phys. Rev. C **63**, 034006 (2001) applies FSI corrections to J. Becker *et al.*, Eur. Phys. J. A **6**, 329 (1999).
 [6] I. Passchier *et al.*, Phys. Rev. Lett. **82**, 4988 (1999).
 [7] H. Zhu *et al.*, Phys. Rev. Lett. **87**, 081801 (2001).
 [8] S. Galster, H. Klein, K. H. Schmidt, D. Wegener, and J. Bleckwenn, Nucl. Phys. B **32**, 221 (1971).
 [9] R. Schiavilla and I. Sick, Phys. Rev. C **64**, 041002 (2001).
 [10] A. I. Akhiezer and M. P. Rekalo, Sov. J. Part. Nucl. **4**, 277 (1974).
 [11] R. G. Arnold, C. E. Carlson, and F. Gross, Phys. Rev. C **23**, 363 (1981).
 [12] H. Arenhövel, Phys. Lett. B **199**, 13 (1987); H. Arenhövel, private communication (2002).
 [13] G. G. Ohlsen and P. W. Keaton, Jr., Nucl. Instr. and Meth. **109**, 41 (1973).
 [14] H. Arenhövel, W. Leidemann, and E. L. Tomusiak, Phys. Rev. C **52**, 1232 (1995); Phys. Rev. C **46**, 455 (1992); Z. Phys. A **331**, 123 (1988); Z. Phys. A **334**, 363(E) (1989); H. Arenhövel, private communication (2002, 2003).
 [15] R. Machleidt, K. Holinde, and Ch. Elster, Phys. Rep. **149**, 1 (1987).
 [16] R. B. Wiringa, V. G. J. Stoks, and R. Schiavilla, Phys. Rev. C **51**, 38 (1995).
 [17] S. Kopecky *et al.*, Phys. Rev. C **56**, 2229 (1997); Phys. Rev. Lett. **74**, 2427 (1995).
 [18] M. Hauger *et al.*, Nucl. Instr. and Meth. A **462**, 382 (2001).
 [19] A. Afanasev, I. Akushevich, and N. Merenkov, Phys. Rev. D **64**, 113009 (2001).
 [20] J. J. Kelly, Phys. Rev. C **66**, 065203 (2002).
 [21] P. Markowitz *et al.*, Phys. Rev. C **48**, R5 (1993).
 [22] E. E. W. Bruins *et al.*, Phys. Rev. Lett. **75**, 21 (1995).
 [23] W. Xu *et al.*, Phys. Rev. C **67**, 012201 (2003).
 [24] J. Friedrich and T. Walcher, hep-ph/0303054.
 [25] G. Kubon *et al.*, Phys. Lett. B **524**, 26 (2002).
 [26] B. D. Milbrath *et al.*, Phys. Rev. Lett. **80**, 452 (1998); Phys. Rev. Lett. **82**, 2221(E) (1999).
 [27] M. K. Jones *et al.*, Phys. Rev. Lett. **84**, 1398 (2000); V. Punjabi *et al.*, (submitted to Phys. Rev. C).
 [28] Th. Pospischil *et al.*, Eur. Phys. J. A **12**, 125 (2001).
 [29] O. Gayou *et al.*, Phys. Rev. Lett. **88**, 092301 (2002).
 [30] G. Holzwarth, hep-ph/020138; Z. Phys. A **356**, 339 (1996). [Version B2 is shown in Fig. 4.]
 [31] B.-Q. Ma, D. Qing, and I. Schmidt, Phys. Rev. C **65**, 035205 (2002).
 [32] S. Boffi, L. Ya. Glozman, W. Klink, W. Plessas, M. Radici, and R. F. Wagenbrunn, Eur. Phys. J. A **14**, 17 (2002); M. Radici, private communication (2002).
 [33] G. A. Miller, Phys. Rev. C **66**, 032201(R) (2002); G. A. Miller, private communication (2002).
 [34] F. Cardarelli and S. Simula, Phys. Rev. C **62**, 065201 (2000); S. Simula, private communication (2002).
 [35] E. L. Lomon, Phys. Rev. C **66**, 045501 (2002); Phys. Rev. C **64**, 035204 (2001).